Design and Analysis of High k_t^2 Shear Horizontal Wave Resonators

Yushuai Liu*†‡, Kangfu Liu*†‡ and Tao. Wu*†‡
Email: liuysh2@shanghaitech.edu.cn; liukf@shanghaitech.edu.cn; wutao@shanghaitech.edu.cn
*School of Information Science and Technology, ShanghaiTech University, Shanghai, China
†Shanghai Institute of Microsystem and Information Technology, Chinese Academy of Sciences, Shanghai, China
‡University of Chinese Academy of Sciences, Beijing, China
⁑Shanghai Engineering Research Center of Energy Efficient and Custom AI IC, Shanghai, China

***Abstract*—The paper demonstrates the design, analysis and of shear horizontal fundamental mode (SH0) resonator based on 36Y-cut Lithium Niobate ($LiNbO_3$) thin film. A spurious-free SH0 resonator response with a k_t^2 of approximately 20.7% has been achieved at the wave propagating orientation of 0° in the 36Y-cut plane. Such a high electromechanical enables the large bandwidth of acoustic-based RF filters.**

Keywords—lithium niobate ($LiNbO_3$), resonator, high coupling coefficient, shear horizontal wave

I. Introduction

Internet of Things (IoTs) has inspired recent studies on low-power and miniature size for applications where wireless functions are event-driven [1]. Recently, voltage controlled oscillator (VCO) and wake-up radio receiver based on microelectromechanical system (MEMS) acoustic resonators have been demonstrated with low power and miniature size [2, 3]. Acoustic resonators as a component of these devices need to exhibit high electromechanical coupling coefficient (k_t^2), high quality factor (Q). Recently, there have been some significant progress in the resonators based on lithium niobate ($LiNbO_3$) film, which can achieve high electromechanical coupling coefficient (k_t^2) and high quality factor Q, simultaneously. For example, the fundamental symmetric (S0) lamb mode of X-cut $LiNbO_3$ typically has an $k_t^2 > 10\%$, and A1 lamb mode resonator shows $k_t^2 > 25\%$. Although S0 mode and A1 mode have been proved to be large k_t^2, the measurement response of S0 mode resonator generally has serious spurious modes around the resonance frequency due to the influence of the non-perpendicular etching angle and the imperfect period; and the resonant frequency (f_s) of the A1 mode resonator is almost determined by the $LiNbO_3$ thickness (h), and can hardly leverage by the interdigital transducer (IDT) pitch.

Shear horizontal (SH) mode on $LiNbO_3$ film provides high k_t^2 thanks to the large piezoelectric coefficient of $LiNbO_3$, attracts wide attention recently. As the optimized cut angle around 30YX $LiNbO_3$ can provide intrinsic coefficient K^2 over 50%. However, spurious modes in their response have deep influence on their entrance to the commercial marketplace. Spurious modes can produce ripples in the pass-band and out-of-band spurious response. Some studies have focused on spurious modes of SH0 modes and worked on the suppression of the spurious modes. Suppression techniques for transverse spurious modes in SH0 X-cut $LiNbO_3$ have been developed using modified edge shapes [8], [9] and length-controlled electrode configurations [8], [10]. Theory analysis has been done to help thoroughly understand the origin of spurious modes in high-order SH0 modes [8]. As known, $LiNbO_3$ is a highly anisotropic material with numerous available cuts via the ion slicing technique. However, the same researches haven't been seen yet aimed at higher-order SH0 spurious modes suppressing in the 36Y-cut $LiNbO_3$. 36Y-cut $LiNbO_3$ cut plane is shown in Fig. 1 (a). The rotated e-matrix is shown in fig. 1 (b) at which e_{16} maximizes. 36Y-cut has the big advantage in e_{16} compared with other cuts of $LiNbO_3$ [11]. So, it can be excited the high k_t^2 in SH0 with top-only interdigitated transducers (IDT).

In this work, 3D finite element analysis (FEA) has been used to analyze the theoretical performance of 36Y-cut $LiNbO_3$ thin-film SH0 mode LVRs, in which the spurious modes are effectively suppressed by properly designing the length and width of the IDT electrodes. The rotated c-matrix is shown in Fig. 1 (c) that can be used in simulation. In addition, the influence of electrode parameters on the coupling coefficient of

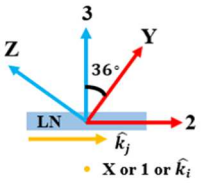

(a)

$$e = \begin{bmatrix} 0 & 0 & 0 & 0 & 0.12 & -4.48 \\ -1.65 & -2.30 & 2.57 & 0.47 & 0 & 0 \\ -1.94 & -1.59 & 4.53 & -0.26 & 0 & 0 \end{bmatrix} C/m^2$$

(b)

$$c = \begin{bmatrix} 202 & 60.3 & 71.9 & -11.2 & 0 & 0 \\ 60.3 & 222 & 90.3 & -8.68 & 0 & 0 \\ 71.9 & 90.3 & 193 & -7.65 & 0 & 0 \\ -11.2 & -8.68 & -7.65 & 75.3 & 0 & 0 \\ 0 & 0 & 0 & 0 & 78.2 & 4.34 \\ 0 & 0 & 0 & 0 & 4.34 & 56.5 \end{bmatrix} Gpa$$

(c)

Fig. 1 (a) Y-Z Plane of the $LiNbO_3$ crystal, showing the cut plane normal to the 36 rotated Y axis; (b) Rotated e-matrix for 36Y-cut $LiNbO_3$; (c) Rotated c-matrix for 36Y-cut $LiNbO_3$;

2021 IEEE International Ultrasonics Symposium (IUS) | 978-1-6654-0355-9/21/$31.00 ©2021 IEEE | DOI: 10.1109/IUS52206.2021.9593617

978-0-7381-1209-1/21/$31.00 ©2021 IEEE

SH0 mode is discussed. Finally, a SH0 mode LVR with a high k_t^2 has been fabricated and characterized.

II. Design and Analysis

A. Suppression of S0 mode lamb wave

The 36Y-cut $LiNbO_3$ has a large piezoelectric stress constant component of -4.48 (C/m^2) in e_{16} shown Fig. 1 (a), which can excite shear horizontal mode easily. The SH0 wave on the bulk material would leak into substrate, which causes losses. And the suspended thin film structure will prevent the leakage into substrate. However, 36Y-cut $LiNbO_3$ also has relatively large e_{31} and e_{33}, which might excite S0 mode on the suspended thin film simultaneously. Under certain h/λ, the frequency of S0 mode will be closed to the main mode enough and causes spurious mode [4]. In order to excite SH0 mode and suppress S0 lamb mode effectively, the influence of the wave propagation direction between both modes was studied. Here, (α, β, γ) were used to represent the Euler rotation angle, for 36Y-cut is (α, -54, 0). The electrode arrangement direction is along the x-axis direction after Euler rotation, then α represents the direction of wave propagation.

Fig. 2 shows the simulated intrinsic coupling coefficient K^2 versus in-plane propagation direction α for the SH0 and S0 mode when h/λ = 0.05, and ignore the thickness of electrode h_e = 0. The K^2 is defined as:

$$K^2 = \frac{v_0^2 - v_m^2}{v_0^2} \quad (1)$$

Where v_0 and v_m represent the open and short surface phase velocity, respectively. As show in Fig. 2, SH0 mode has a maximum value of K^2 when α = 0, while S0 is almost 0. Therefore, the S0 mode can be suppressed, while the SH0 mode can be excited efficiently when α=0. The intrinsic coupling K^2 of SH0 mode is up to 46% in this case.

B. Suppression of high-order SH0 spurious mode

Several studies of the suppression of the spurious mode in piezoelectric resonator [5-7], where longitudinal and transverse indicate the direction along and perpendicular to the propagation direction. Conventional electrode configuration for SH0 mode is shown in Fig. 3 (a), where W and L are the width and length of the suspended plate; W_e and W_p represent the width of the electrode, pitch; L_o and λ are the length of overlap and wavelength, respectively. Neglecting the in-plane an-isotropic, the resonant frequencies of all the acoustic mode in a plate can be expressed by [6]:

$$\hat{k}_{ij} = \hat{k}_i + \hat{k}_j = \frac{2\pi}{\lambda_i}\hat{k}_i + \frac{2\pi}{\lambda_j}\hat{k}_j \quad (1)$$

$$\lambda_i = \frac{2W}{i}, \lambda_j = \frac{2W}{j} \quad (2)$$

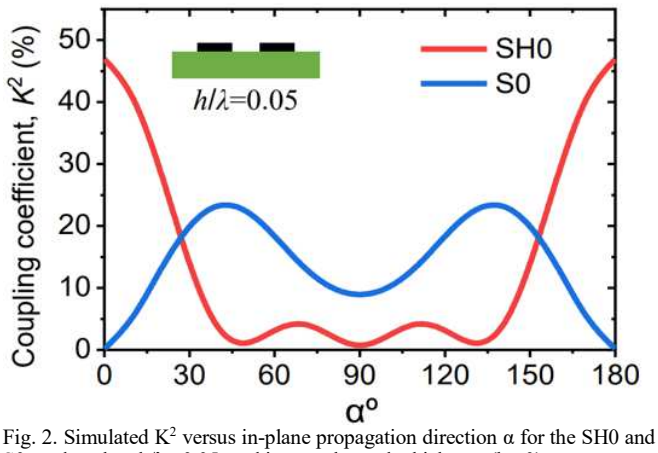

Fig. 2. Simulated K^2 versus in-plane propagation direction α for the SH0 and S0 mode, when h/λ= 0.05, and ignore electrode thickness (h_e=0).

where i and j are the wave vector of the longitudinal and transverse modes, v_0' is the phase velocity of the acoustic wave. For a device with N electrodes, $f_{N-1,1}$ is the desired main mode.

The simulations with different electrode length are analyzed by COMSOL. We set W_e/W_p=50%. k_t^2 of $f_{1,3}$ and $f_{1,1}$ have been calculated. $f_{1,1}$ is our desired mode and $f_{1,3}$ is spurious mode. From Table 1, we can conclude that smaller L will cause extra loss. However, larger L will have the significant gravity effect, causing the stress of the $LiNbO_3$ film to be unbearable and the failure of the device after releasing the resonator structure. Therefore, we select 100 um as the resonator length.

Ignore the effects of the length of electrodes. For a resonator with a number of electrodes (more than 2), many spurious modes occur at different frequencies. When the number of electrodes increases, the higher-order longitudinal modes ($\hat{k}_{(N+1),1}, \hat{k}_{(N+3),1}$ ...) are often positioned closer to the desired mode ($\hat{k}_{(N-1),1}$). The minimum number of interdigitated electrodes (N=2) would make the value of Δf largest as shown in Fig. 4. When the number of figures N = 2, the main mode would distance from and attenuate higher order transverse mode to the most extent, consequently create the largest spurious free space for it. Therefore, to suppress the high-order transverse mode, the electrodes is divided into multiple groups, with only 2 electrodes in each group, and connect the groups parallely, which is shown in Fig. 3 (b). In order to keep $k_{1,1}$ away from $k_{1,3}$ as much as possible, the alternative method is to increase W or decrease L.

Table 1. The simulated K_T^2 of $f_{1,1}$ and $f_{1,3}$ with different electrode length

Electrode L(um)	k_t^2 of $f_{1,1}$	k_t^2 of $f_{1,3}$
80	3.3%	21.0%
90	8.7%	17.0%
100	17.5%	8.5%
110	22.8%	4.8%

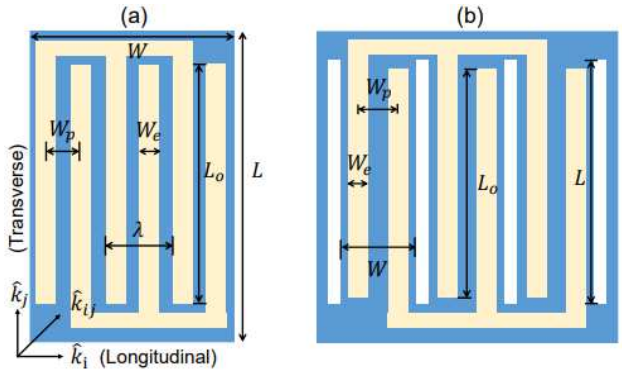

Fig. 3. Electrode configuration in (a) conventional (b) multiple groups.

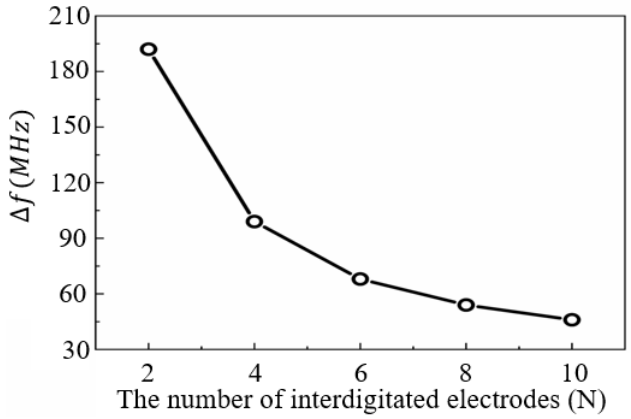

Fig. 4. Simulated resonator frequencies Δf with different number of electrodes. Δf represents the frequency between the fundamental mode $\hat{k}_{N-1,1}$ and high-order longitudinal modes $\hat{k}_{N+1,1}$.

To visualize the displacement mode shapes of shear horizontal modes of various orders, COMSOL finite element analysis (FEA) is used to simulate the eigen modes in a 3D $LiNbO_3$ models shown in Fig. 5. Various order modes from the first ($\hat{k}_{1,1}$) to the fifh ($\hat{k}_{9,1}$) are shown with a mode order denoting the number of half-wavelength periodicities in the longitudinal direction.

However, these two methods have drawbacks, increasing W would reduces fs, and too small L will cause extra losses, since more SH wave will be leaked to surrounding. Therefore, L is setting to be 100 μm, which is a compromise of the film stress, static capacitance and wave leakage. The simulated admittance curves with different pitch are shown in Fig. 6, when n = 2, h = 0.75 μm, L = 100 μm, L_o = 90 μm, h_e = 0.2 μm and W_e/W_p = 50%. $k_{1,1}$ and $k_{1,3}$ are labeled on the curved when W_p = 10 μm, as an example. As expected, with the pitch increases, $k_{1,3}$ is getting far away from the desired $k_{1,1}$, and the coupling coefficient of the spurious mode is decreasing.

C. Coverage

An important factor affecting the coupling is the coverage of the electrode, which expressed as W_e/W_p. This phenomenon does not seem to have been mentioned. We try to give a qualitative explanation: Because the surface where covered by metal is harder to be distorted compare to the free surface, with coverage increase, the hindrance effect of the metal to waves

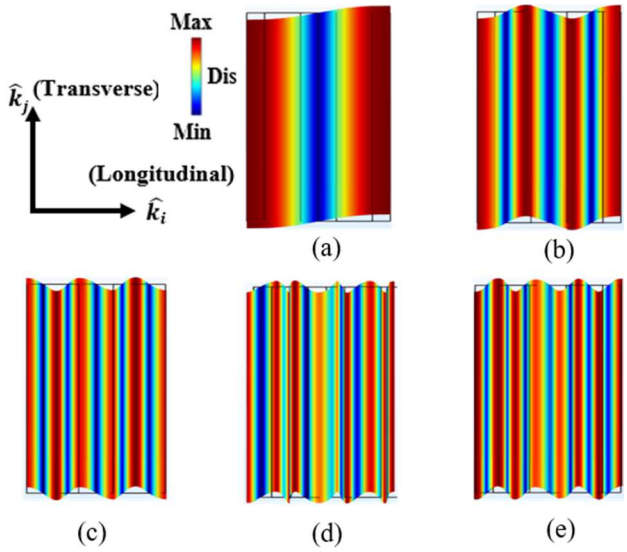

Fig. 5. Displacement high-order SH0 longitudinal mode shapes of the (a) first-order ($\hat{k}_{1,1}$), (b) 2nd-order ($\hat{k}_{3,1}$), (c) 3rd-order ($\hat{k}_{5,1}$), (d) 4th-order ($\hat{k}_{7,1}$), (e) 5th-order ($\hat{k}_{9,1}$)

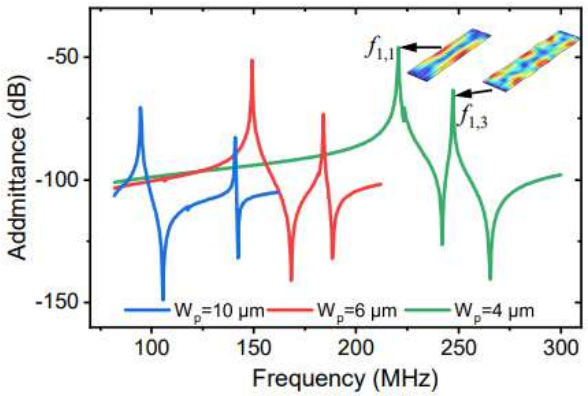

Fig. 6. Simulated admittance with pitch Wp setting as 4, 6 and 10 μm, respectively, while n = 2, h = 0.75 μm, L = 100 μm, L_o = 90 μm, h_e = 0.2 μm and W_e/W_p = 50%

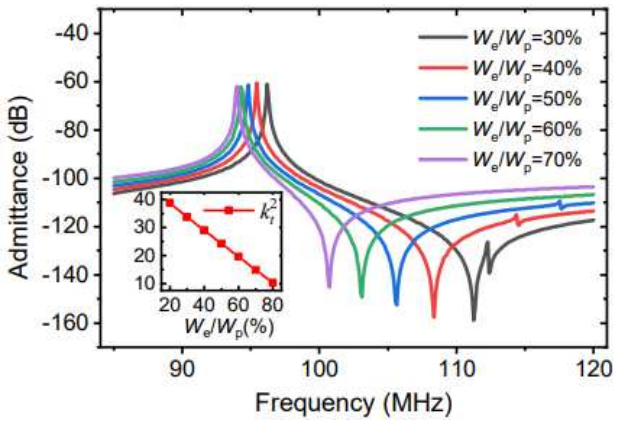

Fig. 7. Simulated admittance under different coverage W_e/W_p, while n = 2, W_p = 10 μm, h = 0.75 μm, L = 100 μm, L_o = 90 μm, h_e = 0.2 μm. The inset shows corresponding k_t^2 with different W_e/W_p.

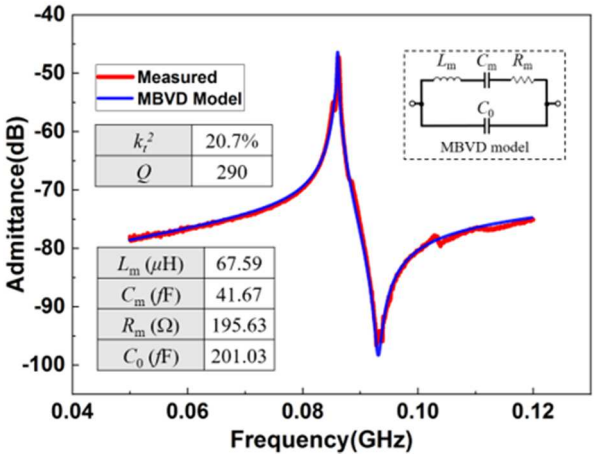

Fig. 8: Measured admittance response of (a) 8 resonators in parallel (M=8, N=2, Electrode length=120 um, Electrode width= 3 um, Electrodes pitch=10 um). (b) The measured circuit modeled response of SH fundamental mode ($\hat{k}_{1,1}$) and MBVD circuit model.

will increase, resulting in a reduction in the coupling of the device. Considering the machining accuracy and the suppression of the parasitic mode, we use W_p = 10 µm for the analysis of coverage.

Fig. 7 shows the simulated admittance under different coverage W_e/W_p, while n = 2, W_p = 10 µm, h = 0.75 µm, L = 100 µm, L_o = 90 µm, h_e = 0.2 µm. The inset shows corresponding k_t^2 with different W_e/W_p. As shown in the inset of Fig. 6, with the coverage increase from 20% to 80%, the coupling coefficient k_t^2 drops from nearly 40% to 10%. It is worth mentioning that with greater the W_p, more degradation of the coupling. The electromechanical coupling coefficient k_t^2 are defined as [8]:

$$k_t^2 = \frac{\pi^2}{8}\frac{f_p^2 - f_s^2}{f_s^2} = \frac{\pi^2}{8}\frac{C_m}{C_0} \quad (3)$$

where f_s and f_p represent the series and parallel resonant frequency, and C0 and Cm is the static and motional capacitance in Modified Butterworth Van Dyke (MBVD) model as shown in Fig. 8.

By the analysis of the theoretical performance of 36Y-cut $LiNbO_3$ thin-film SH0 mode LVRs, the designed fabricated device has shown that the spurious modes can be effectively suppressed by properly designing the length and width of the IDT electrodes as shown in fig. 8. It can achieve the large k_t^2 of 20.7%

III. Conclusions

This work analyzes the theoretical performance of 36Y cut $LiNbO_3$ based devices through finite element simulation. By configuring the length and width of the IDT electrode, the spurious mode is suppressed efficiently. In addition, the influence of electrode coverage and electrodes pitch on the coupling coefficient coverage on the coupling are verified. The fabricated 2-electrode resonator arrays based 36Y-cut $LiNbO_3$ has a high k_t^2 of 20.7%.

Acknowledgments

The authors appreciate the support from the Natural Science Foundation of Shanghai (19ZR1477000) and National Natural Science Foundation of China (61874073). And the authors also appreciate the device fabrication support from ShanghaiTech Quantum Device Lab (SQDL) and Soft Material Nanofabrication Laboratory (SNL).

References

[1] R. H. Olsson, R. B. Bogoslovov, and C. Gordon, "Event driven persistent sensing: Overcoming the energy and lifetime limitations in unattended wireless sensors," in *2016 IEEE SENSORS*, 2016: IEEE, pp. 1-3.

[2] R. Lu, T. Manzaneque, Y. Yang, and S. Gong, "Exploiting parallelism in resonators for large voltage gain in low power wake up radio front ends," in *2018 IEEE Micro Electro Mechanical Systems (MEMS)*, 2018: IEEE, pp. 747-750.

[3] A. Kourani *et al.*, "A 150 MHz voltage controlled oscillator using lithium niobate RF-MEMS resonator," in *2017 IEEE MTT-S International Microwave Symposium (IMS)*, 2017: IEEE, pp. 1307-1310.

[4] J. Zou, V. Yantchev, F. Iliev, V. Plessky, and P. J. Turner, "Ultra-Large-Coupling and Spuriou-Free SH0 Plate Acoustic Wave Resonators based on thin LiNbO3," *IEEE Transactions on Ultrasonics Ferroelectrics and Frequency Control,* vol. PP, no. 99, pp. 1-1, 2019.

[5] Y. H. Song and S. Gong, "Arraying SH0 Lithium Niobate laterally vibrating resonators for mitigation of higher order spurious modes," in *IEEE International Conference on Micro Electro Mechanical Systems*, 2016.

[6] Y. H. Song and S. Gong, "Wideband Spurious-Free Lithium Niobate RF-MEMS Filters," *Journal of Microelectromechanical Systems,* vol. PP, no. 4, pp. 1-9, 2017.

[7] J. Zou, J. Liu, and G. Tang, "Transverse Spurious Mode Compensation for AlN Lamb Wave Resonators," *IEEE Access,* vol. 7, pp. 67059-67067, 2019.

[8] S. Shao, Z. Luo, and T. Wu, "High Figure-of-Merit Lamb Wave Resonators Based on Al0. 7Sc0. 3N Thin Film," *IEEE Electron Device Letters,* vol. 42, no. 9, pp. 1378-1381, 2021.